Bounds for Scattering from Absorptionless Electromagnetic Structures

Rahul Trivedi,[1,2,*] Guillermo Angeris,[1,2] Logan Su,[1] Stephen Boyd,[2] Shanhui Fan,[1,2] and Jelena Vučković[1,2]

[1] *E. L. Ginzton Laboratory, Stanford University, Stanford, California 94305, USA*
[2] *Department of Electrical Engineering, Stanford University Stanford, California 94305, USA*

(Received 6 March 2020; revised 11 May 2020; accepted 26 May 2020; published 9 July 2020)

The design of the scattering properties of electromagnetic structures is of fundamental interest in optical science and engineering. While there has been great practical success in applying local optimization methods to electromagnetic device design, it is unclear whether the performance of the resulting designs is close to that of the best possible design. This question remains open for absorptionless electromagnetic devices, since the absence of material loss makes it difficult to provide provable bounds on their scattering properties. We resolve this problem by providing nontrivial lower bounds on performance metrics that are convex functions of the scattered fields. Our bounding procedure relies on accounting for a constraint on the electric fields inside the device, which can be provably constructed for devices with small footprints or low dielectric contrast. We illustrate our bounding procedure by upper bounding the scattering cross sections of lossless dielectric and metallic particles.

DOI: 10.1103/PhysRevApplied.14.014025

I. INTRODUCTION

An understanding of the scattering properties of electromagnetic structures is a problem of fundamental importance in optical science and engineering. Optimization-based design of electromagnetic devices [1] has enabled device functionalities and performances that are far beyond previously anticipated limits [2–17]. However, even with the application of such sophisticated design methodologies, the fundamental constraint of Maxwell's equations makes arbitrary device functionalities unlikely. This has raised the question of how to calculate rigorous bounds on the performance achievable by optical devices within a given footprint or for a certain set of design materials.

The calculation of bounds on electromagnetic scattering is an old problem—there has been great interest in bounding absorption and scattering in subwavelength electromagnetic structures due to their diverse applications in imaging, biomedicine, and antenna-design [18–21]. Single-frequency properties of electromagnetic fields have traditionally been hard to bound and the bounds present in the existing literature can be broadly classified into three categories:

(a) *Bounds relying on the presence of material absorption*: If the electromagnetic structures being considered have material losses, energy-conservation constraints have been used to provide bounds on their scattering properties [22]. More recently, $\mathbb{T}$-operator formalism has been used to provide rigorous bounds on scattering from subwavelength particles [23–26]. Furthermore, accounting for the cooperative effects of radiation and absorption in electromagnetic scatterers has improved such scattering bounds [27].

(b) *Bounds relying on approximate scattering models*: For absorptionless electromagnetic scattering, bounds on frequency-domain properties, such as the antenna quality factor, directivity, and gain, of electrically small antennas, have been provided based on equivalent-circuit models for the radiated fields [28–32]. While these bounds have been very important in the design of antenna structures, they are not valid when the structure size is comparable to the wavelength of the radiated fields. Furthermore, even for electrically small structures, these bounds rely on the electromagnetic structures radiating into homogeneous media and fail to account for radiation into more complicated media (such as waveguide structures). Channel-counting arguments [33,34] can also be used to provide bounds on scattering cross sections provided that assumptions on the position of resonances of the electromagnetic structures are made.

(c) *Bounds on frequency-integrated scattering properties*: Rigorous bounds on frequency-integrated extinction cross sections for structures of all sizes have been provided using sum rules based on the polarizability dyadics of the structure [35,36] but these fail to bound single-frequency performance without additional assumptions on

*rtrivedi@stanford.edu

the frequency response of the electromagnetic structure. Bounds on frequency-averaged performance of absorptionless electromagnetic structures have also been provided based on analytical continuation of Maxwell's equations [37] but these bounds are very loose if single-frequency performance is of interest.

More recently, lower bounds on error in the electric fields produced by an absorptionless electromagnetic structure relative to a target electric field have been computed by a direct application of Lagrangian duality [38] but this procedure requires the target field to be specified at all points within the design. It thus fails to bound functions of the scattered field that are typically of interest in practical design problems.

In this paper, we consider single-frequency scattering from absorptionless electromagnetic devices and lower-bound frequency-domain performance metrics that can be expressed as convex functions of the scattered fields. Our bounding procedure builds on the principle of Lagrange duality [39,40] and is constructed from Maxwell's equations without any additional assumptions. While a direct application of Lagrange duality to the resulting design problem gives trivial bounds, we show that adding a constraint on the norm of the field inside the electromagnetic device resolves this issue. For low-contrast or subwavelength scatterers, we construct such a constraint from Maxwell's equations and use it to compute bounds on the performance of the device. As an application of this bounding procedure, we use it to calculate upper limits on the scattering cross section of a two-dimensional (2D) absorptionless electromagnetic scatterer.

II. FORMALISM

Figure 1 shows the considered setup: a lossless electromagnetic device in a design region Γ is embedded in a background structure with permittivity distribution $\varepsilon_b(\mathbf{x})$. The composition and geometry of the electromagnetic device is described by its contrast $\chi(\mathbf{x})$ relative to the background permittivity distribution, i.e., the permittivity distribution inside Γ is given by $\varepsilon(\mathbf{x}) = \varepsilon_b(\mathbf{x}) + \chi(\mathbf{x})$. Under excitation by an incident field $\mathbf{E}_{\text{inc}}(\mathbf{x})$ propagating in the background medium $\varepsilon_b(\mathbf{x})$, the electric field $\mathbf{E}(\mathbf{x})$ inside the design region Γ can be computed from

$$\mathbf{E}(\mathbf{x}) = \mathbf{E}_{\text{inc}}(\mathbf{x}) + \hat{G}_b \mathbf{\Phi}(\mathbf{x}), \quad \forall \mathbf{x} \in \Gamma, \tag{1}$$

where $\hat{G}_b$ is the Green's function of the background structure and $\mathbf{\Phi}(\mathbf{x}) = \chi(\mathbf{x})\mathbf{E}(\mathbf{x})$ is the polarization current inside the design region. The fields scattered from the device, $\mathbf{E}_{\text{sca}}(\mathbf{x})$, are the fields radiated by the polarization current $\mathbf{\Phi}(\mathbf{x})$. Throughout this paper, except for the scattered fields $\mathbf{E}_{\text{sca}}(\mathbf{x})$, all vector fields are only defined within Γ. Furthermore, we will assume the following definition of the inner product $\langle \cdot, \cdot \rangle$ of two such vector fields, $\mathbf{V}(\mathbf{x})$ and $\mathbf{U}(\mathbf{x})$:

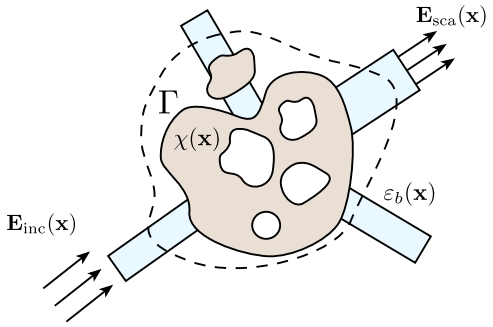

FIG. 1. A schematic showing an electromagnetic device within the region Γ with contrast $\chi(\mathbf{x})$ embedded in an electromagnetic background with permittivity distribution $\varepsilon_b(\mathbf{x})$, excited with an incident electromagnetic field $\mathbf{E}_{\text{inc}}(\mathbf{x})$ to produce a scattered field $\mathbf{E}_{\text{sca}}(\mathbf{x})$.

$$\langle \mathbf{V}, \mathbf{U} \rangle = \int_{\Gamma} \mathbf{V}^*(\mathbf{x}) \cdot \mathbf{U}(\mathbf{x})\, d^3\mathbf{x}, \tag{2}$$

with the usual definition of the norm: $\|\mathbf{V}\| = \sqrt{\langle \mathbf{V}, \mathbf{V} \rangle}$.

In a typical optical design problem, we wish to optimize a performance metric (e.g., transmission through an output port of the device, or the scattering cross section of the device) with respect to the contrast within the design region. Optimization of many such performance metrics can be mapped to minimization of convex functions of $\mathbf{E}_{\text{sca}}(\mathbf{x})$ and consequently as convex functions of $\mathbf{\Phi}(\mathbf{x})$, since $\mathbf{E}_{\text{sca}}(\mathbf{x})$ is linear in $\mathbf{\Phi}(\mathbf{x})$. Assuming that the contrast is restricted to vary between two specified limits χ_- and χ_+, the optimal contrast $\chi_{\text{opt}}(\mathbf{x})$, its electric field $\mathbf{E}_{\text{opt}}(\mathbf{x})$, polarization current $\mathbf{\Phi}_{\text{opt}}(\mathbf{x})$, and performance f_{opt} can be obtained by solving the following optimization problem:

$$\begin{aligned} \underset{\mathbf{\Phi},\mathbf{E},\chi \in [\chi_-,\chi_+]}{\text{minimize}} \quad & f\,[\mathbf{\Phi}] \\ \text{subject to} \quad & \mathbf{E}(\mathbf{x}) = \mathbf{E}_{\text{inc}}(\mathbf{x}) + \hat{G}_b \mathbf{\Phi}(\mathbf{x}), \quad \forall \mathbf{x} \in \Gamma, \\ & \mathbf{\Phi}(\mathbf{x}) = \chi(\mathbf{x})\mathbf{E}(\mathbf{x}), \quad \forall \mathbf{x} \in \Gamma, \end{aligned} \tag{3}$$

where f captures the performance metric. While there has been great success in locally solving this nonconvex optimization problem using gradient-based optimization techniques together with adjoint sensitivity analysis, it is hard to solve it globally and exactly calculate f_{opt}.

One approach to lower bound such a nonconvex optimization problem is to use Lagrange duality [39,40], which constructs a convex, and thus globally solvable, optimization problem that lower bounds the original nonconvex problem. The first step in the application of Lagrangian duality is to construct the Lagrangian $\mathcal{L}$ by adding the

constraints in problem (3) to the objective function:

$$\mathcal{L}[\mathbf{\Phi},\mathbf{E},\chi;\mathbf{V},\mathbf{S}] = f[\mathbf{\Phi}] + 2\mathrm{Re}\left[\left\langle \mathbf{V}, \mathbf{E}-\mathbf{E}_{\mathrm{inc}}-\hat{G}_b\mathbf{\Phi}\right\rangle\right] + 2\mathrm{Re}\left[\langle \mathbf{S}, \mathbf{\Phi}-\chi\mathbf{E}\rangle\right]. \quad (4)$$

Here, we have introduced vector fields $\mathbf{V}(\mathbf{x})$ and $\mathbf{S}(\mathbf{x})$ defined within the design region Γ, often referred to as the *dual variables*, corresponding to the constraints $\mathbf{E}(\mathbf{x}) = \mathbf{E}_{\mathrm{inc}}(\mathbf{x}) + \hat{G}_b\mathbf{\Phi}(\mathbf{x})$ and $\mathbf{\Phi}(\mathbf{x}) = \chi(\mathbf{x})\mathbf{E}(\mathbf{x})$, respectively. Since $(\mathbf{\Phi}_{\mathrm{opt}}, \mathbf{E}_{\mathrm{opt}}, \chi_{\mathrm{opt}})$ satisfy the constraints in problem (3), it follows from Eq. (4) that

$$\mathcal{L}[\mathbf{\Phi}_{\mathrm{opt}}, \mathbf{E}_{\mathrm{opt}}, \chi_{\mathrm{opt}}; \mathbf{V}, \mathbf{S}] = f[\mathbf{\Phi}_{\mathrm{opt}}] = f_{\mathrm{opt}}. \quad (5)$$

The *dual function* $g[\mathbf{V},\mathbf{S}]$ is defined as

$$g[\mathbf{V},\mathbf{S}] = \inf_{\mathbf{\Phi},\mathbf{E},\chi\in[\chi_-,\chi_+]} \mathcal{L}[\mathbf{\Phi},\mathbf{E},\chi;\mathbf{V},\mathbf{S}]. \quad (6)$$

We note that while constructing $g[\mathbf{V},\mathbf{S}]$, we minimize $\mathcal{L}$ over all possible values of $\mathbf{\Phi}, \mathbf{E}$, and $\chi \in [\chi_-, \chi_+]$ instead of only those that satisfy the constraints in problem (3). Since the set of all possible $(\mathbf{\Phi}, \mathbf{E}, \chi)$ also includes $(\mathbf{\Phi}_{\mathrm{opt}}, \mathbf{E}_{\mathrm{opt}}, \chi_{\mathrm{opt}})$, it immediately follows from Eqs. (5) and (6) that $g[\mathbf{V},\mathbf{S}] \le f_{\mathrm{opt}}\ \forall\ \mathbf{V},\mathbf{S}$. The best lower bound that $g[\mathbf{V},\mathbf{S}]$ can provide is obtained by maximizing it with respect to the dual variables $\mathbf{V}$ and $\mathbf{S}$. It can be shown that maximizing $g[\mathbf{V},\mathbf{S}]$ is a convex optimization problem despite the original problem (3) being nonconvex [39].

The dual function $g[\mathbf{V},\mathbf{S}]$ in Eq. (6) can be analytically calculated using Eq. (4)—as shown in Appendix A:

$$g[\mathbf{V},\mathbf{S}] = \begin{cases} -f^\star[0], & \text{if } \mathbf{V}(\mathbf{x}) = 0 \text{ and } \mathbf{S}(\mathbf{x}) = 0,\ \forall \mathbf{x}\in\Gamma \\ -\infty, & \text{otherwise.} \end{cases} \quad (7)$$

where $f^\star$ is the Fenchel dual of f given by Ref. [40]

$$f^\star[\mathbf{N}] = \sup_{\mathbf{\Phi}} \left(2\mathrm{Re}[\langle \mathbf{N}, \mathbf{\Phi}\rangle] - f[\mathbf{\Phi}]\right). \quad (8)$$

From this, it immediately follows that $\sup_{\mathbf{V},\mathbf{S}} g[\mathbf{V},\mathbf{S}] = \min_{\mathbf{\Phi}} f[\mathbf{\Phi}]$. Thus, the bound obtained is the minimum value of the performance metric f in problem (3) without accounting for Maxwell's equations, i.e., use of the dual function corresponding to the Lagrangian in Eq. (4) results in a trivial bound.

The key insight to resolving this issue is to note that the fields inside the design region cannot be arbitrarily large for most problems of interest. Therefore, we first consider a restriction of this problem where the norm of the difference between the electric field $\mathbf{E}(\mathbf{x})$ and a reference field $\mathbf{E}_{\mathrm{ref}}(\mathbf{x})$ is constrained to be

$$\|\mathbf{E}-\mathbf{E}_{\mathrm{ref}}\| \le \alpha\|\mathbf{E}_{\mathrm{ref}}\|. \quad (9)$$

Here, α is a dimensionless parameter that controls the magnitudes of the fields inside Γ. The reference field $\mathbf{E}_{\mathrm{ref}}(\mathbf{x})$ can be the electric field for any specific device. The Lagrangian function $\mathcal{L}$ corresponding to problem (3) with this field constraint is given by

$$\mathcal{L}[\mathbf{\Phi},\mathbf{E},\chi;\mathbf{V},\mathbf{S},\lambda] = f[\mathbf{\Phi}] + 2\mathrm{Re}\left[\langle \mathbf{V}, \mathbf{E}-\mathbf{E}_{\mathrm{inc}}-\hat{G}_b\mathbf{\Phi}\rangle\right] + 2\mathrm{Re}\left[\langle \mathbf{S}, \mathbf{\Phi}-\chi\mathbf{E}\rangle\right] + \lambda(\|\mathbf{E}-\mathbf{E}_{\mathrm{ref}}\|^2 - \alpha^2\|\mathbf{E}_{\mathrm{ref}}\|^2), \quad (10)$$

where, compared to Eq. (4), we introduce an additional dual variable $\lambda \ge 0$ for the field constraint. The dual function $g[\mathbf{V},\mathbf{S},\lambda]$ for the Lagrangian in Eq. (10) can then be constructed by minimizing it over $\mathbf{\Phi}, \mathbf{E}$ and $\chi \in [\chi_-, \chi_+]$. As shown in the Appendix B, the optimal dual value $d(\alpha) = \sup_{\mathbf{V},\mathbf{S},\lambda\ge0} g[\mathbf{V},\mathbf{S},\lambda]$, can be computed by solving the following conic program [39,40]:

$$\begin{aligned} \underset{\mathbf{V},\mathbf{S},\beta,\lambda\ge0}{\text{maximize}} \quad & 2\mathrm{Re}\left[\langle \mathbf{V}, \mathbf{E}_{\mathrm{ref}}-\mathbf{E}_{\mathrm{inc}}\rangle\right] - f^\star\left[\mathbf{S}-\hat{G}_b^\dagger\mathbf{V}\right] \\ & - \int_\Gamma \beta(\mathbf{x})\, d^3\mathbf{x} - \lambda\alpha^2\|\mathbf{E}_{\mathrm{ref}}\|^2 \\ \text{subject to} \quad & \beta(\mathbf{x}) \ge \frac{|\mathbf{V}(\mathbf{x}) - \chi_\pm\mathbf{S}(\mathbf{x})|^2}{\lambda} \\ & + 2\chi_\pm\mathrm{Re}\left[\mathbf{S}^*(\mathbf{x})\cdot\mathbf{E}_{\mathrm{ref}}(\mathbf{x})\right], \quad \forall\mathbf{x}\in\Gamma, \end{aligned} \quad (11)$$

where $f^\star$ is the Fenchel dual of f [40]. The solution of the convex problem (11), $d(\alpha)$, then provides a lower bound on the solution of problem (3) subject to the field constraint [Eq. (9)]. From a physical standpoint, $d(\alpha)$ captures how the scattering properties of the scatterer depend on the maximum allowed field intensity inside the design region.

Since problem (3) does not explicitly impose Eq. (9), in order to use the solution of problem (11) to obtain a bound on f_{opt}, it is necessary to choose α such that Eq. (9) will be satisfied for all feasible fields. The smallest α that satisfies this requirement is the optimal solution of the following problem:

$$\begin{aligned} \underset{\mathbf{E},\chi\in[\chi_-,\chi_+]}{\text{maximize}} \quad & \|\mathbf{E}-\mathbf{E}_{\mathrm{ref}}\|/\|\mathbf{E}_{\mathrm{ref}}\| \\ \text{subject to} \quad & \mathbf{E}(\mathbf{x}) = \mathbf{E}_{\mathrm{inc}}(\mathbf{x}) + \hat{G}_b\chi(\mathbf{x})\mathbf{E}(\mathbf{x}), \quad \forall\mathbf{x}\in\Gamma. \end{aligned} \quad (12)$$

Problem (12) is nonconvex and likely difficult to solve globally. However, it follows from Eq. (1) that α_{UB}, defined below, is an upper bound on the solution of problem (12) and hence a valid choice for α in Eq. (9) (for details, see Appendix C):

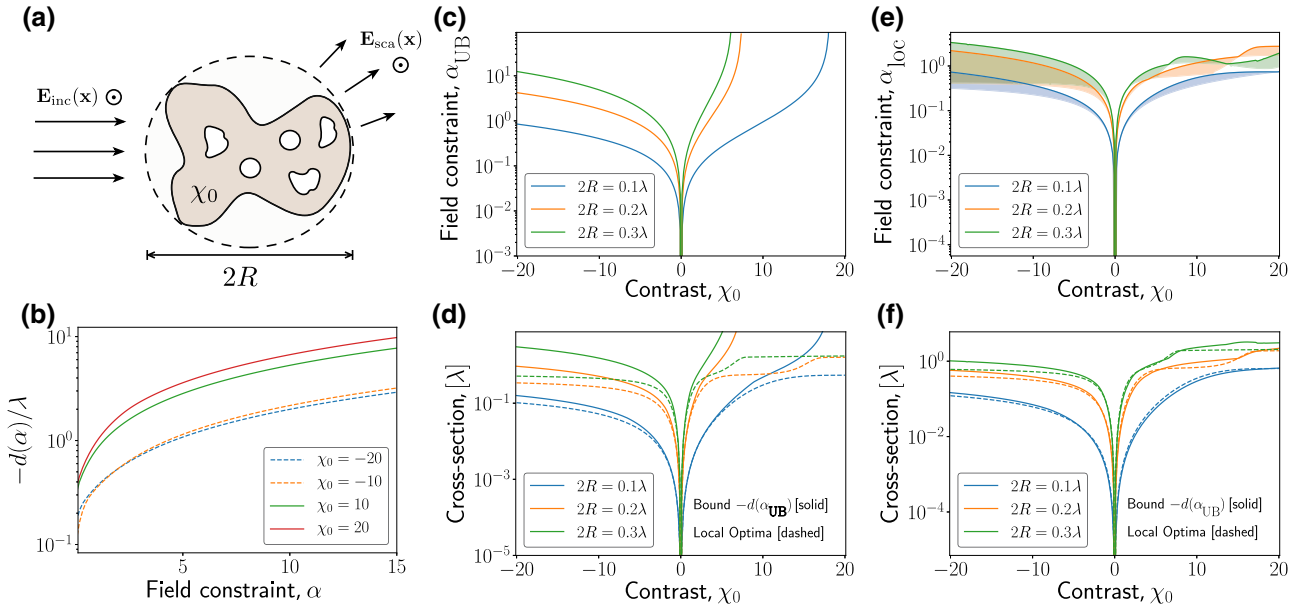

FIG. 2. The TE-scattering cross section. (a) A schematic of the scattering problem. (b) The bound $-d(\alpha)/\lambda$ on the scattering cross section under the field constraint [Eq. (9)] as a function of α for $2R = 0.2\lambda$. (c) The field constraint $\alpha_{\rm UB}$ as a function of contrast χ_0 for different R. (d) The upper bound $-d(\alpha_{\rm UB})$ on the scattering cross section. The locally optimized scattering cross section is shown in dashed lines. (e) The local optimum of problem (12), $\alpha_{\rm loc}$ as a function of the contrast χ_0 for different R. The shaded regions indicate the distribution of local optima obtained with 50 different initial conditions. (f) The solution of problem (11) with $\alpha = \alpha_{\rm loc}$ shown alongside the locally optimized scattering cross sections. In all calculations, the vector fields inside Γ are represented on a square grid with discretization $\delta x = \lambda/100$.

$$\alpha_{\rm UB} = \begin{cases} \dfrac{\|(\hat{I} - \bar{\chi}\hat{G}_b)^{-1}\hat{G}_b\|\delta\chi}{\left[1 - \delta\chi\|(\hat{I} - \bar{\chi}\hat{G}_b)^{-1}\hat{G}_b\|\right]}, & \text{if } \delta\chi\|(\hat{I} - \bar{\chi}\hat{G}_b)^{-1}\hat{G}_b\| < 1 \\ \infty, & \text{otherwise,} \end{cases} \tag{13}$$

where $\bar{\chi} = (\chi_+ + \chi_-)/2$, $\delta\chi = |\chi_+ - \chi_-|/2$ and $\mathbf{E}_{\rm ref}(\mathbf{x}) = (\hat{I} - \bar{\chi}\hat{G}_b)^{-1}\mathbf{E}_{\rm inc}(\mathbf{x})$. Therefore, $d(\alpha_{\rm UB})$ is a lower bound on the optimal value of the nonconvex design problem (3):

$$d(\alpha_{\rm UB}) \leq f_{\rm opt}. \tag{14}$$

It can be noted that $\alpha_{\rm UB}$ and consequently $d(\alpha_{\rm UB})$ depend on the choice of the design region Γ through the background Green's function $\hat{G}_b$ and the limits $\chi_\pm$ on the contrast $\chi(\mathbf{x})$. Furthermore, we note that $d(\alpha_{\rm UB})$ is a nontrivial bound only when the design region Γ, χ_-, and χ_+ are chosen such that $\delta\chi\|(\hat{I} - \bar{\chi}\hat{G}_b)^{-1}\hat{G}_b\| < 1$. While this is a shortcoming of the procedure presented in this paper, an improved upper bound on the optimal value of problem (12) would likely improve the bound $f_{\rm opt}$.

III. EXAMPLE: UPPER BOUND ON SCATTERING CROSS SECTION

As an example, we consider computing upper bounds on the scattering cross section of a 2D lossless scatterer. For this problem, the function f can be chosen to be the negative of the scattering cross section expressed in terms of the polarization current density $\mathbf{\Phi}(\mathbf{x})$: $f[\mathbf{\Phi}] = -2\text{Im}[\langle \mathbf{E}_{\rm inc}, \mathbf{\Phi}\rangle]$. From Eq. (14), it follows that the upper bound on the cross section is $-d(\alpha_{\rm UB})$. Furthermore, to numerically solve problem (11), we discretize the vector fields $[\mathbf{V}(\mathbf{x}), \mathbf{S}(\mathbf{x})]$, the scalar fields $[\beta(\mathbf{x})]$, and the Green's function $(\hat{G}_b)$ using the pulse-basis and delta-testing functions [41]. Numerical studies of the convergence of the discretized problem are included in Appendix D.

We first consider the scattering cross section for a transverse-electric (TE) problem [Fig. 2(a)], where the electric fields are polarized along the z axis while varying

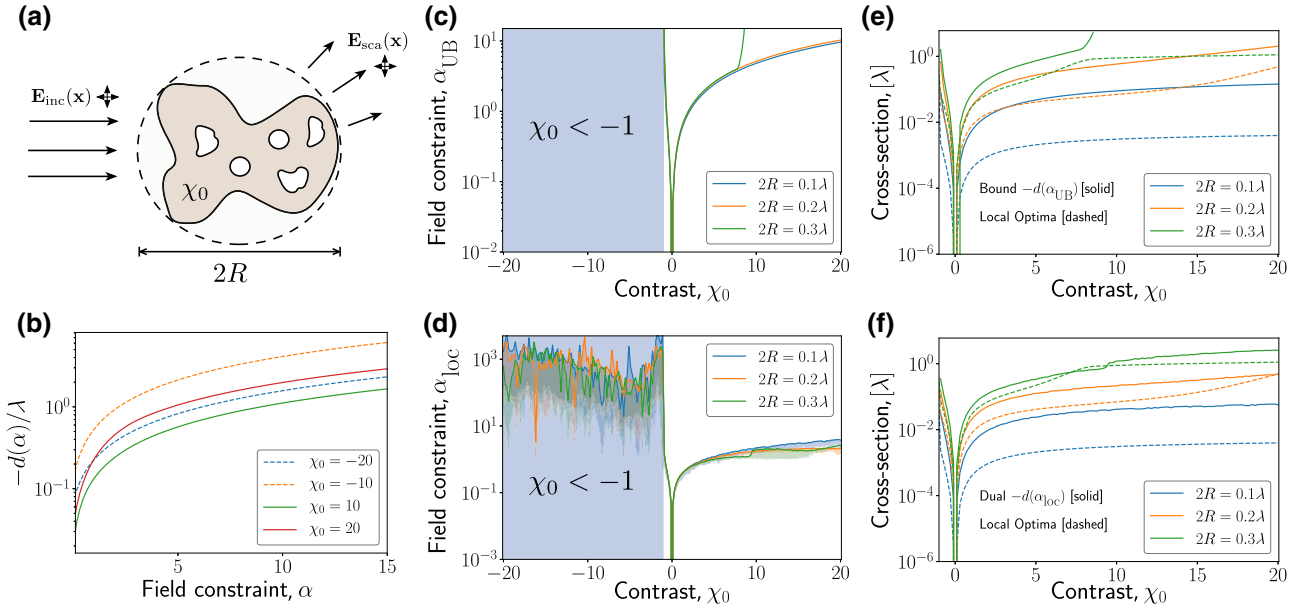

FIG. 3. The TM-scattering cross section. (a) A schematic of the scattering problem. (b) The bound $-d(\alpha)/\lambda$ on the scattering cross section under the field constraint [Eq. (9)] as a function of α for $2R = 0.2\lambda$. (c) The field constraint $\alpha_{\rm UB}$ as a function of the contrast χ_0 for different R. (d) The local optimum of problem (12), $\alpha_{\rm loc}$, as a function of contrast χ_0 for different R. The shaded regions indicate the distribution of local optima obtained with 50 different initial conditions. (e) The upper bound $-d(\alpha_{\rm UB})$ on the scattering cross section. The locally optimized cross section is shown in dashed lines. (f) The solution of problem (11) with $\alpha = \alpha_{\rm loc}$ shown alongside the locally optimized scattering cross sections. In all calculations, the vector fields inside Γ are represented on a square grid with discretization $\delta x = \lambda/100$.

spatially with (x, y). We restrict ourselves to a circular design region of radius R, with contrast $\chi(\mathbf{x})$ varying between 0 and χ_0 and with the background medium being vacuum [$\varepsilon_b(\mathbf{x}) = 1$]. Figure 2(b) shows the upper bound on the scattering cross section under the field constraint Eq. (9) as a function of α, obtained by solving problem (11)—our bounds indicate that allowing for higher fields in the design region allows it to have a larger scattering cross section. Figure 2(c) shows the field bound $\alpha_{\rm UB}$ for the TE-scattering problem. For a given radius of the design region, increasing the magnitude of the contrast χ_0 results in an increase in $\alpha_{\rm UB}$, with $\alpha_{\rm UB} \to \infty$ beyond a cutoff for $\chi_0 > 0$. Interestingly, the field bound $\alpha_{\rm UB}$ does not diverge for negative χ_0. Figure 2(d) shows the bound on the scattering cross section obtained by solving problem (11) with $\alpha = \alpha_{\rm UB}$—the bound (solid) is compared to the result of local optimization of the scattering cross section (dashed). We note that for small values of contrast or for small design regions, our bounds are close to the locally optimized results and significant deviation between the two is only seen due to the divergence in $\alpha_{\rm UB}$.

However, an improved constraint on the fields would likely allow us to provide significantly tighter bound for the scattered fields. This is illustrated in Figs. 2(e) and 2(f), where we locally solve problem (12) to obtain $\alpha_{\rm loc}$, which only approximates problem (12) and hence does not necessarily enforce Eq. (9) for all feasible fields. As can be seen from Fig. 2(e), unlike $\alpha_{\rm UB}$, $\alpha_{\rm loc}$ does not diverge and the corresponding optimal value of $-d(\alpha_{\rm loc})$, while not being an actual bound on the scattering cross section, agrees more closely with the result of locally optimizing the scattering cross section [Fig. 2(f)].

Next, we consider the scattering cross section for a transverse-magnetic (TM) problem [Fig. 3(a)], where the electric fields are polarized in the x-y plane, while varying spatially with (x, y). The choice of the design region and the allowed contrast is identical to that of the TE problem. Figure 3(b) shows the solution of the problem (11) that bounds the scattering cross section under the field constraint [Eq. (9)]—similar to the TE case, we observe that the scattering cross section is bounded provided that the fields inside the scatterers are not allowed to be arbitrarily large. Figure 3(c) shows $\alpha_{\rm UB}$ as a function of the contrast χ_0—in contrast to the TE case, we observe that $\alpha_{\rm UB} \to \infty$ for $\chi_0 \leq -1$ (i.e., if negative permittivities are allowed in the design region) irrespective of the radius of the design region. For positive χ_0, $\alpha_{\rm UB}$ diverges for large χ_0 as indicated in Eq. (13). The divergence of $\alpha_{\rm UB}$ for positive χ_0 is a consequence of the field bounds [Eq. (13)] being loose, while the divergence for negative χ_0 is physical. To provide more evidence for this claim, we locally solve the nonconvex-optimization problem (12) to obtain $\alpha_{\rm loc}$, which approximates α. Figure 3(d) shows $\alpha_{\rm loc}$ as a function of the contrast χ_0 for different

design-region radii R—we note that for negative χ_0, we obtain extremely large values for α_{loc} that are only limited by the spatial discretization used for representing the fields inside the design region Γ, while for positive values of χ_0, we obtain α_{loc} that converges with respect to the spatial discretization (for numerical studies, refer to Appendix E). Consequently, our bounding procedure suggests that the scattering cross section for the TM problem is unbounded if negative-permittivity materials are allowed in the design region and is bounded if the scatterer is composed entirely of positive-permittivity materials [Figs. 3(e) and 3(f)]. This observation is consistent with superscattering effects expected in lossless metallic nanoparticles [42–44] due to the existence of surface-plasmon modes with aligned resonant frequencies.

IV. CONCLUSION

This paper outlines a bounding procedure for absorptionless electromagnetic devices. As an example, we use it to study upper limits on scattering cross sections of 2D electromagnetic metallic and dielectric scatterers. The generality of the bounding procedure makes it an attractive technique to understand fundamental limits for a variety of electromagnetic design problems. Furthermore, while we focus on the problem of bounding fields from absorptionless electromagnetic devices, the procedure outlined in this paper can be integrated with the approaches outlined in Refs. [22–27,31,34] to provide tighter bounds for absorptive electromagnetic devices. Finally, we note that the general techniques introduced in this paper are not specialized to bounding electromagnetic scattering but are easily extendible to wave-scattering problems in other fields such as acoustics or quantum physics.

ACKNOWLEDGMENTS

R.T. acknowledges a Kailath Graduate Fellowship. This work has been supported by the Air Force Office of Scientific Research (AFOSR) Multidisciplinary Research Program of the University Research Initiative (MURI) on attojoule optoelectronics (Grant No. FA9550-17-1-0002) and Samsung. We thank Alexander Y. Piggott for useful discussions and Alex White, Sattwik Deb Mishra, and Geun Ho Ahn for providing feedback on the manuscript.

APPENDIX A: DUAL OF THE ORIGINAL PROBLEM

Here, we construct the dual function $g(\mathbf{V},\mathbf{S})$ corresponding to the Lagrangian in Eq. (4) and show that it provides a trivial bound on the performance metric $f[\mathbf{\Phi}]$ in problem (3). From Eq. (4), it follows that

$$\inf_{\mathbf{\Phi}} \mathcal{L} = -f^\star[\mathbf{S} - \hat{G}_b^\dagger \mathbf{V}] - 2\text{Re}[\langle \mathbf{V}, \mathbf{E}_{\text{inc}} \rangle] + 2\text{Re}[\langle \mathbf{V} - \chi \mathbf{S}, \mathbf{E} \rangle], \tag{A1}$$

where $f^\star$ is the Fenchel dual of f, given by [40]

$$f^\star[\mathbf{N}] = \sup_{\mathbf{\Phi}} \left(2\text{Re}[\langle \mathbf{N}, \mathbf{\Phi} \rangle] - f[\mathbf{\Phi}]\right). \tag{A2}$$

Minimizing Eq. (A1) over $\mathbf{E}$, we obtain

$$\inf_{\mathbf{E},\mathbf{\Phi}} \mathcal{L} = \begin{cases} -f^\star[\mathbf{S} - \hat{G}_b^\dagger \mathbf{V}] - 2\text{Re}[\langle \mathbf{V}, \mathbf{E}_{\text{inc}} \rangle], & \text{if } \mathbf{V}(\mathbf{x}) = \chi(\mathbf{x})\mathbf{S}(\mathbf{x}),\ \forall \mathbf{x} \in \Gamma \\ -\infty, & \text{otherwise} \end{cases} \tag{A3}$$

Finally, $g[\mathbf{V},\mathbf{S}]$ can be obtained by minimizing Eq. (A3) over $\chi \in [\chi_-, \chi_+]$. Note that unless $\mathbf{V}(\mathbf{x}) = 0$ and $\mathbf{S}(\mathbf{x}) = 0$, $\forall \mathbf{x} \in \Gamma$, $\chi(\mathbf{x})$ can always be chosen so as to give $g[\mathbf{V},\mathbf{S}] = -\infty$. Therefore,

$$g[\mathbf{V},\mathbf{S}] = \begin{cases} -f^\star[0], & \text{if } \mathbf{V}(\mathbf{x}) = 0 \text{ and } \mathbf{S}(\mathbf{x}) = 0, \quad \forall \mathbf{x} \in \Gamma \\ -\infty, & \text{otherwise} \end{cases} \tag{A4}$$

As described in the main text, $g[\mathbf{V},\mathbf{S}]$ is a lower bound on the optimal solution f_{opt} in problem (3) for any choice of $\mathbf{V}$ and $\mathbf{S}$. Consequently, maximization of $g[\mathbf{V},\mathbf{S}]$ over $\mathbf{V}$ and $\mathbf{S}$ gives the best lower bound on f_{opt}. It immediately follows from Eqs. (A4) and (A2) that this is given by

$$\sup_{\mathbf{V},\mathbf{S}} g[\mathbf{V},\mathbf{S}] = -f^\star[0] = \inf_{\mathbf{\Phi}} f[\mathbf{\Phi}]. \tag{A5}$$

This bound is simply the smallest value of the performance metric in problem (3) without accounting for its constraints—it is consequently a trivial bound on f_{opt}. It can be noted that for the problem of calculating an upper limit on the scattering cross section that is considered in the main text, Eq. (A5) indicates that the scattering cross section is unbounded irrespective of the choice of design region Γ and the contrast limits $\chi_\pm$.

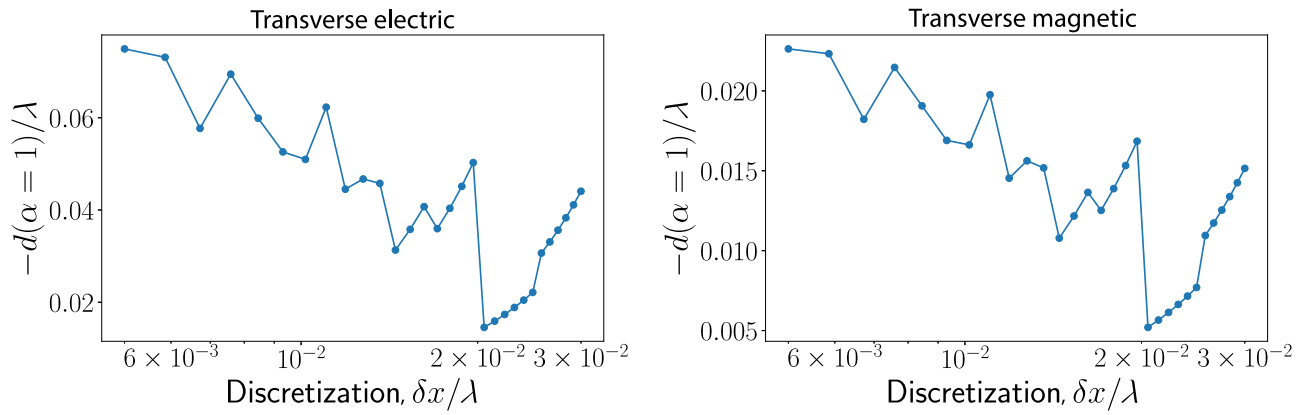

FIG. 4. The solution of problem (11) with the objective function being the 2D TE- and TM-scattering cross sections for different discretization parameters δx. The design region is assumed to be a circle of radius 0.1λ embedded in vacuum and the contrast $\chi_0 = 2.5$.

APPENDIX B: DUAL OF THE FIELD-CONSTRAINED PROBLEM

Here, we outline a brief derivation of the dual problem of the field-constrained problem. Minimizing the Lagrangian in Eq. (10) over $\mathbf{\Phi}(\mathbf{x})$, we obtain

$$\begin{aligned}\inf_{\mathbf{\Phi}} \mathcal{L} = &-f^\star\left[\mathbf{S} - \hat{G}_b^\dagger \mathbf{V}\right] + 2\mathrm{Re}\left[\langle \mathbf{V}, \mathbf{E} - \mathbf{E}_{\mathrm{inc}}\rangle\right] \\ &- 2\mathrm{Re}\left[\langle \mathbf{S}, \chi \mathbf{E}\rangle\right] \\ &+ \lambda\left(\|\mathbf{E} - \mathbf{E}_{\mathrm{ref}}\|^2 - \alpha^2 \|\mathbf{E}_{\mathrm{ref}}\|^2\right).\end{aligned} \tag{B1}$$

Minimizing Eq. (B1) over $\mathbf{E}(\mathbf{x})$, we obtain

$$\begin{aligned}\inf_{\mathbf{E},\mathbf{\Phi}} \mathcal{L} = &\,2\mathrm{Re}\left[\langle \mathbf{V}, \mathbf{E}_{\mathrm{ref}} - \mathbf{E}_{\mathrm{inc}}\rangle\right] - f^\star\left[\mathbf{S} - \hat{G}_b^\dagger \mathbf{V}\right] \\ &- \int_\Gamma \frac{|\mathbf{V}(\mathbf{x}) - \chi(\mathbf{x})\mathbf{S}(\mathbf{x})|^2}{\lambda}\, d^3\mathbf{x} \\ &- 2\mathrm{Re}\left[\langle \mathbf{S}, \chi \mathbf{E}_{\mathrm{ref}}\rangle\right].\end{aligned} \tag{B2}$$

Finally, to calculate the dual function $g[\mathbf{V}, \mathbf{S}, \lambda]$ by minimizing Eq. (B2) over $\chi \in [\chi_-, \chi_+]$, note that $\inf_{\mathbf{E},\mathbf{\Phi}} \mathcal{L}$ is a concave function in $\chi(\mathbf{x})$ and is separable at each point in the domain Γ, so it will acquire its minimum value with respect to $\chi(\mathbf{x})$ at either χ_- or χ_+ $\forall\, \mathbf{x} \in \Gamma$. Consequently,

$$\begin{aligned}g[\mathbf{V}, \mathbf{S}, \lambda] = &\,2\mathrm{Re}\left[\langle \mathbf{V}, \mathbf{E}_{\mathrm{ref}} - \mathbf{E}_{\mathrm{inc}}\rangle\right] - f^\star[\mathbf{S} - \hat{G}_b^\dagger \mathbf{V}] \\ &- \int_\Gamma \beta(\mathbf{x})\, d^3\mathbf{x},\end{aligned} \tag{B3}$$

where

$$\begin{aligned}\beta(\mathbf{x}) = \max_{\chi \in \{\chi_+, \chi_-\}} \Bigg[&\frac{|\mathbf{V}(\mathbf{x}) - \chi \mathbf{S}(\mathbf{x})|^2}{\lambda} \\ &- 2\chi\,\mathrm{Re}\left(\mathbf{S}^*(\mathbf{x}) \cdot \mathbf{E}_{\mathrm{ref}}(\mathbf{x})\right)\Bigg].\end{aligned} \tag{B4}$$

Since $g[\mathbf{V}, \mathbf{S}, \lambda]$ provides a bound on f_{opt} for any choice of $\mathbf{V}, \mathbf{S}$ and $\lambda \geq 0$ [39,40], the best lower bound is then obtained by maximizing it over all the dual variables. This immediately yields the convex optimization problem in the main text [problem (11)]. Except for an explicit introduction of the polarization current $\mathbf{\Phi}(\mathbf{x})$ and the field constraint [Eq. (9)], the calculation of the dual problem outlined in this section is similar to that presented in Ref. [38].

APPENDIX C: CALCULATION OF THE FIELD CONSTRAINT

Here, we show that if $\mathbf{E}_{\mathrm{ref}}(\mathbf{x}) = (\hat{\mathrm{I}} - \bar{\chi}\hat{G}_b)^{-1}\mathbf{E}_{\mathrm{inc}}(\mathbf{x})$, then α_{UB} provided in Eq. (13) provides an upper bound on $\|\mathbf{E} - \mathbf{E}_{\mathrm{ref}}\|$ for all $\mathbf{E}(\mathbf{x})$ that are solutions of Eq. (1) with $\chi_- \leq \chi(\mathbf{x}) \leq \chi_+$ $\forall\, \mathbf{x} \in \Gamma$.

Note that Eq. (1) can be rewritten to obtain

$$\mathbf{E}(\mathbf{x}) - (\hat{I} - \bar{\chi}\hat{G}_b)^{-1}\hat{G}_b[\chi(\mathbf{x}) - \bar{\chi}]\mathbf{E}(\mathbf{x}) = \mathbf{E}_{\mathrm{ref}}(\mathbf{x}). \tag{C1}$$

It immediately follows from the reverse triangle inequality and Eq. (C1) that

$$\|\mathbf{E}\| - \|(\hat{I} - \bar{\chi}\hat{G}_b)^{-1}\hat{G}_b(\chi - \bar{\chi})\mathbf{E}\| \leq \|\mathbf{E}_{\mathrm{ref}}\|. \tag{C2}$$

Furthermore, $\|(\hat{I} - \bar{\chi}\hat{G}_b)^{-1}\hat{G}_b(\chi - \bar{\chi})\mathbf{E}\| \geq \|(\hat{I} - \bar{\chi}\hat{G}_b)^{-1}\hat{G}_b\| \cdot \|(\chi - \bar{\chi})\mathbf{E}\|$, where $\|(\hat{I} - \bar{\chi}\hat{G}_b)^{-1}\hat{G}_b\|$ is the operator norm of $(\hat{I} - \bar{\chi}\hat{G}_b)^{-1}\hat{G}_b$. Furthermore, since $\chi_- \leq \chi(\mathbf{x}) \leq \chi_+$ $\forall$ $\mathbf{x} \in \Gamma$, it follows that $|\chi(\mathbf{x}) - \bar{\chi}| \leq \delta\chi$ $\forall\, \mathbf{x} \in \Gamma$ where $\delta\chi = |\chi_+ - \chi_-|/2$. Consequently, from Eq. (C2), we immediately obtain

$$\left[1 - \left\|\left(\hat{I} - \bar{\chi}\hat{G}_b\right)^{-1}\hat{G}_b\right\|\delta\chi\right]\|\mathbf{E}\| \leq \|\mathbf{E}_{\mathrm{ref}}\|. \tag{C3}$$

Clearly, if $\|(\hat{I} - \bar{\chi}\hat{G}_b)^{-1}\hat{G}_b\|\delta\chi < 1$, it follows that $\|\mathbf{E}\|$ is bounded above by $\|\mathbf{E}_{\mathrm{ref}}\|/[1 - \|(\hat{I} - \bar{\chi}\hat{G}_b)^{-1}\hat{G}_b\|\delta\chi]$.

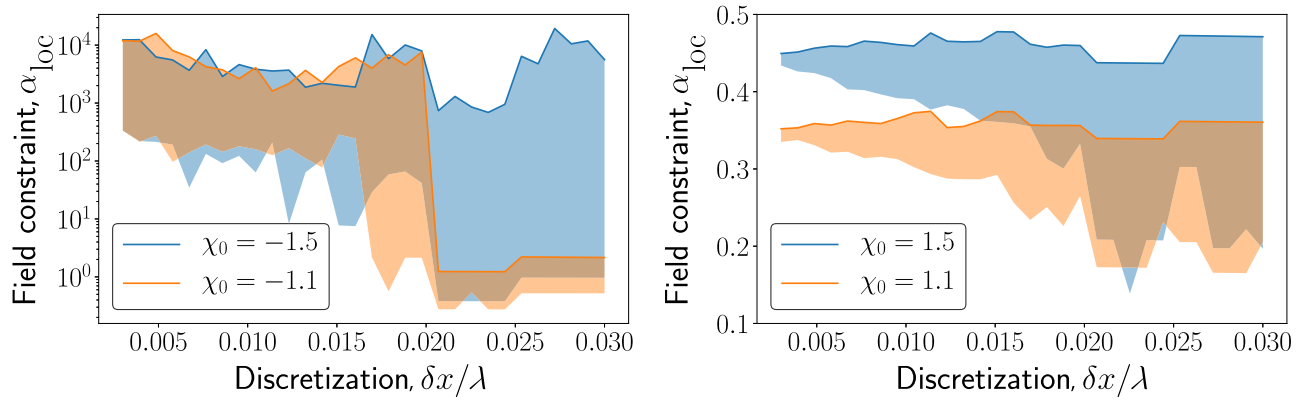

FIG. 5. The field constraint α_{loc} obtained by locally solving the nonconvex problem in problem (12) as a function of the discretization parameter δx. The shaded regions indicate the range of local optima obtained by solving the nonconvex problem with 50 different initial conditions. A circular design region with radius 0.1λ embedded in vacuum is assumed in all calculations.

From Eq. (C1), this bound can easily be translated to a bound on $\|\mathbf{E} - \mathbf{E}_{\text{ref}}\|$:

$$\|\mathbf{E} - \mathbf{E}_{\text{ref}}\| = \|(\hat{I} - \bar{\chi}\hat{G}_b)^{-1}\hat{G}_b(\chi - \bar{\chi})\mathbf{E}\| \leq \frac{\|(\hat{I} - \bar{\chi}\hat{G}_b)^{-1}\hat{G}_b\|\delta\chi\|\mathbf{E}_{\text{ref}}\|}{1 - \|(\hat{I} - \bar{\chi}\hat{G}_b)^{-1}\hat{G}_b\|\delta\chi}. \quad \text{(C4)}$$

If $\|(\hat{I} - \bar{\chi}\hat{G}_b)^{-1}\hat{G}_b\|\delta\chi \geq 1$, then the procedure outlined above cannot be used to generate a bound on $\|\mathbf{E} - \mathbf{E}_{\text{ref}}\|$.

APPENDIX D: NUMERICAL CONVERGENCE OF THE DUAL PROBLEM

In order to solve problem (11), all the involved vector fields need to be discretized within the device region Γ. Furthermore, to ensure that the bounds produced by this problem are not numerical artifacts of the discretization, it is necessary to ensure that the bounds converge with respect to the discretization parameter. This is shown in Fig. 4—the discretization parameter δx refers to the length of the pixels used for representing the design region Γ for the 2D scattering problems using pulse-basis and delta-testing functions [41].

APPENDIX E: DIVERGENCE OF FIELD BOUND

Figure 5 shows locally optimized solutions of problem (12), α_{loc}, for a TM-scattering problem as a function of the discretization parameter δx. We clearly see that for $\chi_0 < -1$, α_{loc} does not converge on reducing δx, while for $\chi_0 > -1$, it converges.

[1] Sean Molesky, Zin Lin, Alexander Y. Piggott, Weiliang Jin, Jelena Vucković, and Alejandro W. Rodriguez, Inverse design in nanophotonics, Nat. Photonics **12**, 659 (2018).

[2] Logan Su, Alexander Y. Piggott, Neil V. Sapra, Jan Petykiewicz, and Jelena Vuckovic, Inverse design and demonstration of a compact on-chip narrowband three-channel wavelength demultiplexer, ACS Photonics **5**, 301 (2018).

[3] Alexander Y. Piggott, Eric Y. Ma, Logan Su, Geun Ho Ahn, Neil V. Sapra, Dries J. F. Vercruysse, Andrew M. Netherton, Akhilesh S. P. Khope, John E. Bowers, and Jelena Vučković, Inverse-designed photonics for semiconductor foundries, arXiv:1911.03535 (2019).

[4] Logan Su, Rahul Trivedi, Neil V. Sapra, Alexander Y. Piggott, Dries Vercruysse, and Jelena Vučković, Fully-automated optimization of grating couplers, Opt. Express **26**, 4023 (2018).

[5] Alexander Y. Piggott, Jan Petykiewicz, Logan Su, and Jelena Vučković, Fabrication-constrained nanophotonic inverse design, Sci. Rep. **7**, 1 (2017).

[6] Neil V. Sapra, Dries Vercruysse, Logan Su, Ki Youl Yang, Jinhie Skarda, Alexander Y. Piggott, and Jelena Vučković, Inverse design and demonstration of broadband grating couplers, IEEE J. Sel. Top. Quantum Electron. **25**, 1 (2019).

[7] Zin Lin, Adi Pick, Marko Lončar, and Alejandro W. Rodriguez, Enhanced Spontaneous Emission at Third-Order Dirac Exceptional Points in Inverse-Designed Photonic Crystals, Phys. Rev. Lett. **117**, 107402 (2016).

[8] Chawin Sitawarin, Weiliang Jin, Zin Lin, and Alejandro W. Rodriguez, Inverse-designed photonic fibers and metasurfaces for nonlinear frequency conversion, Photonics Res. **6**, B82 (2018).

[9] Zin Lin, Benedikt Groever, Federico Capasso, Alejandro W. Rodriguez, and Marko Lončar, Topology-Optimized Multilayered Metaoptics, Phys. Rev. Appl. **9**, 044030 (2018).

[10] Weiliang Jin, Sean Molesky, Zin Lin, Kai-Mei C. Fu, and Alejandro W. Rodriguez, Inverse design of compact multimode cavity couplers, Opt. Express **26**, 26713 (2018).

[11] Jacob Andkjær, Villads Egede Johansen, Kasper Storgaard Friis, and Ole Sigmund, Inverse design of nanostructured surfaces for color effects, JOSA B **31**, 164 (2014).

[12] Jesper Riishede and Ole Sigmund, Inverse design of dispersion compensating optical fiber using topology optimization, JOSA B **25**, 88 (2008).

[13] Søren Halkjær, Ole Sigmund, and Jakob S. Jensen, Inverse design of phononic crystals by topology optimization, Z. Kristallographie-Crystalline Mater. **220**, 895 (2005).
[14] Tyler W. Hughes, Momchil Minkov, Ian A. D. Williamson, and Shanhui Fan, Adjoint method and inverse design for nonlinear nanophotonic devices, ACS Photonics **5**, 4781 (2018).
[15] Tyler Hughes, Georgios Veronis, Kent P. Wootton, R. Joel England, and Shanhui Fan, Method for computationally efficient design of dielectric laser accelerator structures, Opt. Express **25**, 15414 (2017).
[16] David Sell, Jianji Yang, Sage Doshay, Rui Yang, and Jonathan A. Fan, Large-angle, multifunctional metagratings based on freeform multimode geometries, Nano Lett. **17**, 3752 (2017).
[17] Jianji Yang and Jonathan A. Fan, Topology-optimized metasurfaces: Impact of initial geometric layout, Opt. Lett. **42**, 3161 (2017).
[18] Shuming Nie and Steven R. Emory, Probing single molecules and single nanoparticles by surface-enhanced Raman scattering, Science **275**, 1102 (1997).
[19] Javier Aizpurua, Pl Hanarp, D. S. Sutherland, M. Käll, Garnett W. Bryant, and F. J. Garcia De Abajo, Optical Properties of Gold Nanorings, Phys. Rev. Lett. **90**, 057401 (2003).
[20] Andrea Alù and Nader Engheta, Multifrequency Optical Invisibility Cloak with Layered Plasmonic Shells, Phys. Rev. Lett. **100**, 113901 (2008).
[21] Jon A. Schuller, Thomas Taubner, and Mark L. Brongersma, Optical antenna thermal emitters, Nat. Photonics **3**, 658 (2009).
[22] Owen D. Miller, Athanasios G. Polimeridis, M. T. Homer Reid, Chia Wei Hsu, Brendan G. DeLacy, John D. Joannopoulos, Marin Soljačić, and Steven G. Johnson, Fundamental limits to optical response in absorptive systems, Opt. Express **24**, 3329 (2016).
[23] Sean Molesky, Pengning Chao, and Alejandro W. Rodriguez, $\mathbb{T}$-operator limits on electromagnetic scattering: Bounds on extinguished, absorbed, and scattered power from arbitrary sources, arXiv:2001.11531 (2020).
[24] Prashanth S. Venkataram, Sean Molesky, Weiliang Jin, and Alejandro W. Rodriguez, Fundamental Limits to Radiative Heat Transfer: The Limited Role of Nanostructuring in the Near-Field, Phys. Rev. Lett. **124**, 013904 (2020).
[25] Sean Molesky, Prashanth S. Venkataram, Weiliang Jin, and Alejandro W. Rodriguez, Fundamental limits to radiative heat transfer: Theory, Phys. Rev. B **101**, 035408 (2020).
[26] Sean Molesky, Weiliang Jin, Prashanth S. Venkataram, and Alejandro W. Rodriguez, $\mathbb{T}$-Operator Bounds on Angle-Integrated Absorption and Thermal Radiation for Arbitrary Objects, Phys. Rev. Lett. **123**, 257401 (2019).
[27] Zeyu Kuang, Lang Zhang, and Owen D. Miller, Maximal single-frequency electromagnetic response, arXiv:2002.00521 (2020)s.
[28] Lan Jen Chu, Physical limitations of omni-directional antennas, J. Appl. Phys. **19**, 1163 (1948).
[29] H. Thal, Exact circuit analysis of spherical waves, IEEE Trans. Antennas Propag. **26**, 282 (1978).
[30] Harold A. Wheeler, Fundamental limitations of small antennas, Proc. IRE **35**, 1479 (1947).
[31] Do-Hoon Kwon and David M. Pozar, Optimal characteristics of an arbitrary receive antenna, IEEE Trans. Antennas Propag. **57**, 3720 (2009).
[32] James S. McLean, A re-examination of the fundamental limits on the radiation Q of electrically small antennas, IEEE Trans. Antennas Propag. **44**, 672 (1996).
[33] Rafif E. Hamam, Aristeidis Karalis, J. D. Joannopoulos, and Marin Soljačić, Coupled-mode theory for general free-space resonant scattering of waves, Phys. Rev. A **75**, 053801 (2007).
[34] Zongfu Yu, Aaswath Raman, and Shanhui Fan, Fundamental limit of nanophotonic light trapping in solar cells, Proc. Natl. Acad. Sci. **107**, 17491 (2010).
[35] Mats Gustafsson, Christian Sohl, and Gerhard Kristensson, Physical limitations on antennas of arbitrary shape, Proc. R. Soc. A: Math. Phys. Eng. Sci. **463**, 2589 (2007).
[36] Mats Gustafsson, Christian Sohl, and Gerhard Kristensson, Illustrations of new physical bounds on linearly polarized antennas, IEEE Trans. Antennas Propag. **57**, 1319 (2009).
[37] Hyungki Shim, Lingling Fan, Steven G. Johnson, and Owen D. Miller, Fundamental Limits to Near-Field Optical Response over any Bandwidth, Phys. Rev. X **9**, 011043 (2019).
[38] Guillermo Angeris, Jelena Vuckovic, and Stephen P. Boyd, Computational bounds for photonic design, ACS Photonics **6**, 1232 (2019).
[39] Stephen Boyd, Stephen P. Boyd, and Lieven Vandenberghe, *Convex Optimization* (Cambridge University Press, Cambridge, United Kingdom, 2004).
[40] Dimitri P. Bertsekas, Nonlinear programming, J. Oper. Res. Soc. **48**, 334 (1997).
[41] Andrew F. Peterson, Scott L. Ray, Raj Mittra, Institute of Electrical, and Electronics Engineers, *Computational Methods for Electromagnetics* (IEEE Press, New York, 1998), Vol. 1.
[42] Zhichao Ruan and Shanhui Fan, Superscattering of Light from Subwavelength Nanostructures, Phys. Rev. Lett. **105**, 013901 (2010).
[43] Zhichao Ruan and Shanhui Fan, Design of subwavelength superscattering nanospheres, Appl. Phys. Lett. **98**, 043101 (2011).
[44] Ali Mirzaei, Andrey E. Miroshnichenko, Ilya V. Shadrivov, and Yuri S. Kivshar, Superscattering of light optimized by a genetic algorithm, Appl. Phys. Lett. **105**, 011109 (2014).